Pergamon

Int. J. Heat Mass Transfer. Vol. 38, No. 9, pp. 1565–1576, 1995

0017-9310/95 $9.50 + 0.00

0017-9310(94)00292-4

Effect of material composition and localized heat generation on time-dependent conjugate heat transport

J. S. NIGEN and C. H. AMON†

Department of Mechanical Engineering and Engineering Design Research Center, Carnegie Mellon University, Pittsburgh, PA 15213, U.S.A.

(*Received* 8 *February* 1994 *and in final form* 28 *August* 1994)

Abstract—Time-dependent conjugate conduction/convection direct numerical simulations of four rib configurations that differ in material composition and distribution of internal heat generation are conducted in laminar and transitional grooved-channel flows. The effect of material composition, concentration of heat generation and flow regime on the spatial distribution of temperature, heat flux and Nusselt number along the solid–fluid interface is investigated. Furthermore, the distribution of internal heat generation is found to affect strongly the convective resistance at the solid–fluid interface of the rib, leading to a non-monotonic relationship between convective heat transport and Reynolds number for the range of parameters investigated in the configurations with local heat generation.

INTRODUCTION

Thermal phenomena have served as limiting constraints in the design and operation of equipment used in a variety of industries, such as aerospace, energy production, automotive and, recently, electronics. In such circumstances, the maximum temperature experienced by critical components is constrained to prevent thermally-induced failures that result from fatigue, melting and variations in material properties. Should the naturally-present heat transport prove inadequate to prevent these failure modes, augmentation techniques or additional heat exchangers are employed. These heat exchangers can either be detached systems, such as the radiator in an automobile, or integrated into a component, such as cooling passages within turbine blades or heat spreaders within electronic packages. For these configurations, heat is generated internally and/or at solid–fluid interfaces and is then transferred to the environment by a combination of heat transfer modes from and within the system or component. A thermal resistance is associated with each transport mode, representing the induced temperature drop for a fixed energy flux. Therefore, the thermal design problem involves reducing the thermal resistance(s) associated with mode(s) of heat transfer to minimize the induced temperature drops and thermal gradients.

The thermal resistance associated with heat conduction can be reduced by using more conductive materials and by improving the contact conductivity associated with any subcomponent interfaces. However, these approaches can result in prohibitively high manufacturing costs. Alternatively, the amount of convective transport can be increased through additional surface area, thinning of the boundary layers, and homogenization of the temperature distribution within the cooling fluid. The latter can be achieved by increasing the Reynolds number to obtain transitional or turbulent flows and with turbulators or flow destabilizers. However, these approaches result in additional pressure drop that increases operating expenses.

The problem confronting the heat transfer engineer is to determine an adequate cooling design that balances performance with manufacturing and operating expenses. An ill-conceived thermal design can either be ineffective, thereby degrading the life span of a system, or over-designed, adding unnecessary size, weight and expense. It is therefore essential to accurately analyze the thermal performance of a system. However, the competitive environment of today's marketplace limits the time available for analysis and design. These stringent time constraints may require the thermal engineer to neglect less significant effects while developing system models.

Often, the thermal modeling procedure reduces analysis to solving the heat equation within the solid domain. Convective effects, associated with the environmental fluid, are imposed through the heat transfer coefficient at the solid–fluid boundaries. Correlations for heat transfer coefficients have been empirically generated for a variety of geometries and flow conditions. However, most correlations have been obtained with the use of either spatially-uniform temperature or heat flux boundary conditions. In essence, the effect of heat conduction within the solid is replaced by idealized boundary conditions, which

† Author to whom correspondence should be addressed.

NOMENCLATURE

c_p	specific heat
h	heat transfer coefficient $= Q/(T_{s-f} - T_{bulk})$
H	half-channel height
k	thermal conductivity
$\mathbf{n}$	outward normal with respect to solid surface
Nu	Nusselt number $= (hH)/k_f$
p	pressure
Q	heat flux
Re	Reynolds number $= (3VH)/(2\nu)$
t	time
T	temperature
u'''	internal heat generation
$\mathbf{v}$	velocity
V	channel-averaged velocity.

Greek symbols

α	thermal diffusivity
ν	kinematic viscosity
ρ	density
ω	vorticity.

Subscripts

bulk	bulk-mean temperature at leading edge of the rib
f	fluid
s	solid
s–f	solid–fluid interface.

presuppose the heat flow paths within the solid. Therefore, the resistances associated with conduction within the solid and convection within the fluid have been decoupled, an assumption that may not be appropriate for all systems.

The coupling of conduction within the solid and convection within the fluid, termed conjugation, is required in the analysis of systems that involve intense heat transfer, multimaterial solid domains and localized heat generation, as described by Perelman [1]. In conjugate problems, neither the temperature nor the heat flux at solid–fluid interfaces can be prescribed *a priori*. Therefore, the convective boundary condition, as previously described, may not be accurate. The appropriate boundary conditions are continuity of heat flux and temperature at the solid–fluid interface and are termed boundary conditions of the fourth kind.

Analytical conjugate studies of external flows over flat plates have been conducted using either assumed velocity profiles or Blassius boundary layer solutions with uniform heat generation [1–4] and constant temperature along one surface of the plate [5]. Poiseuille flows in circular and planar pipes of finite thickness, accounting for viscous dissipation, have also been studied [2]. Furthermore, Luikov [5] analytically developed heat transfer correlations for conjugate problems that involve functions of a spatially-variable Biot number, called the Brun number. A more recent analytical work involves conjugate heat transfer for a single-material, uniformly heated block [6]. Conjugate heat transfer through a variable-thickness wall was analyzed using variational calculus, demonstrating that the minimum heat flux through the wall is obtained when the wall thickness diminishes in the streamwise flow direction [7]. Unfortunately, all the resulting descriptions of temperature, heat flux and convective transport distributions tend to be rather complex, rendering them difficult to implement in a design setting. Furthermore, most systems are not well modeled by single-material, uniform heat generating solid domains, thereby limiting the applicability of these works.

Numerical studies provide an alternative and, sometimes, a unique approach for configurations with non-homogeneous solid domains. A two-dimensional steady conjugate study of a system with a multimaterial solid domain and a heat source at the solid–fluid interface was conducted using finite differences [8]. The time-dependent conjugate behavior of a semi-infinite slab [9] and slab-wall configuration [10] exposed to uniform surface heating was studied using the unsteady surface element method. The two-dimensional conjugate behavior of hydrodynamically fully-developed, laminar flow through a circular tube with thick walls and a finite heated length was investigated using a finite volume approach [11]. Recent interest in electronics cooling has fostered research on conjugate heat transfer from simulated electronic components. A finite-volume based approach was used to study the steady-state, conjugate behavior of three single-material, uniform heat generating blocks [12] and one multimaterial, local heat generating electronic component [13]. A semi-analytical approach that utilizes an integral formulation for the fluid domain and a finite volume formulation for the solid domain was successfully developed to study plates with discrete heat sources, which model surface-mounted electronic packages [14]. Mixed laminar convection from multimaterial, local heat generating components was also studied using a simpler-based approach [15]. Time-dependent studies of multimaterial, local heat generating configurations using the spectral element method were conducted by Nigen and Amon [16, 17] for both laminar and transitional Reynolds numbers. This investigation contrasted thermal behavior characteristics for conjugate and convection-only representations of a simulated electronic package and demonstrated the significance of including time-dependency and conjugation.

In each of the previous studies, conjugation was found to affect thermal performance characteristics. However, only parameters such as material composition and Reynolds number were independently varied to assess their relative effect upon temperature, flux and heat transport. The purpose of this study is to explore the fundamental effect of the distribution of internal heat generation and multimaterial composition on conjugate heat transfer in grooved channels over a range of laminar and transitional Reynolds numbers, for it is important to consider the relative contribution of non-homogeneity within the solid domain and concentration of heat generation to develop accurate thermal models. Furthermore, some systems may require combined reduction of thermal resistances associated with multiple modes of heat transfer to achieve optimum, or near optimum, cooling designs. Therefore, the following four representative configurations are investigated: (1) local heat generation with single-material composition (LS); (2) local heat generation with multimaterial composition (LM); (3) uniform heat generation with single-material composition (US); and (4) uniform heat generation with multimaterial composition (UM).

PROBLEM FORMULATION

The mathematical model of a conjugate conduction/convection problem with incompressible flow involves a system of partial differential equations for the solid and fluid domains [equations (1)–(3)]. The fluid properties are assumed constant and buoyancy forces are neglected, as well as viscous dissipation and radiation:

$$\frac{\partial \mathbf{v}}{\partial t} = \mathbf{v} \times \boldsymbol{\omega} - \frac{1}{\rho} \nabla \left(p + \frac{\rho v^2}{2} \right) + \nu \nabla^2 \mathbf{v} \tag{1}$$

$$\nabla \cdot \mathbf{v} = 0 \tag{2}$$

$$\frac{\partial T}{\partial t} = \alpha \nabla^2 T - \mathbf{v} \cdot \nabla T + \frac{u'''}{\rho c_p}. \tag{3}$$

The boundary conditions for the momentum equation are no slip along the solid–fluid interfaces and periodicity in the streamwise direction (Fig. 1). For the energy equation, the top surface of the upper wall and the bottom surface of the lower wall are adiabatic, and periodicity is imposed in the streamwise direction by subtracting the calculated rise in mixed-mean temperature on a point-by-point basis at each streamwise location.

The numerical procedure employed for the spatial discretization is the spectral element technique [18, 19]. The spatial domain is decomposed into macro-elements, upon which tensor products of high-order Legendre polynomials are projected. The elemental discretization used is shown in Fig. 2(a) and the mesh indicating the distribution of internal nodes is shown in Fig. 2(b). The control of spatial resolution and the high degree of accuracy associated with this technique makes it well suited for studying time-dependent conjugate problems with localized heat generation and multimaterial solid domains, especially those with large disparities in material properties.

The accuracy of the spectral element solution may be affected either by increasing the total number of macro-elements, obtaining algebraic convergence, or by increasing the order of the local expansions, achieving nearly-exponential convergence. Adequate resolution was verified by comparing the flow characteristics using both seventh- and ninth-order local expansions, as well as using different macro-elemental discretizations. The results from the simulations for the macro-elemental discretization used in this study with seventh- and ninth-order expansions yielded virtually identical results, indicating that the lower resolution was adequate for this investigation.

The numerical approach is to integrate the continuity and momentum equations for the fluid domain and then the energy equation for both the solid and fluid domains. This procedure is iterated in time, using a three-step, semi-implicit, time-splitting scheme, until either a steady or time-periodic state is reached. A typical mesh consisting of 198 macro-elements, each containing 49 degrees of freedom, requires 3.14 s CPU per time step on a Cray Y-MP.

The dimensions and composition of the solid domain, as shown in Fig. 1, represent a typical electronic package. The material properties and, when appropriate, the associated amount of heat generation, are displayed in Table 1. The thermal conductivities displayed in Table 1 include contact resistance, which is modeled by modifying the conductivity, such that the effective thermal resistance obtained is commensurate with empirical data from Yovanovich and Antonetti [20].

It should be noted that, because buoyancy effects are neglected, the resulting flow patterns are independent of the solid–fluid interface temperature and heat flux distributions. Therefore, for a specific Reynolds number, the variations present in the distributions of surface temperature, heat flux, and Nusselt number are only attributable to the composition of the solid domain and the distribution of heat generation. It is this combination, along with the local-fluid characteristics, which determines the heat flow paths and, ultimately, the thermal performance characteristics of the configuration.

FLOW PATTERNS

Three Reynolds numbers are considered for this investigation: low, middle and high. The low Reynolds number case corresponds to a laminar flow field, wherein the fluid in the channel is separated by a shear layer from the recirculating fluid within the groove [16]. Figure 3(a) displays the contours of the streamfunction corresponding to the laminar flow regime

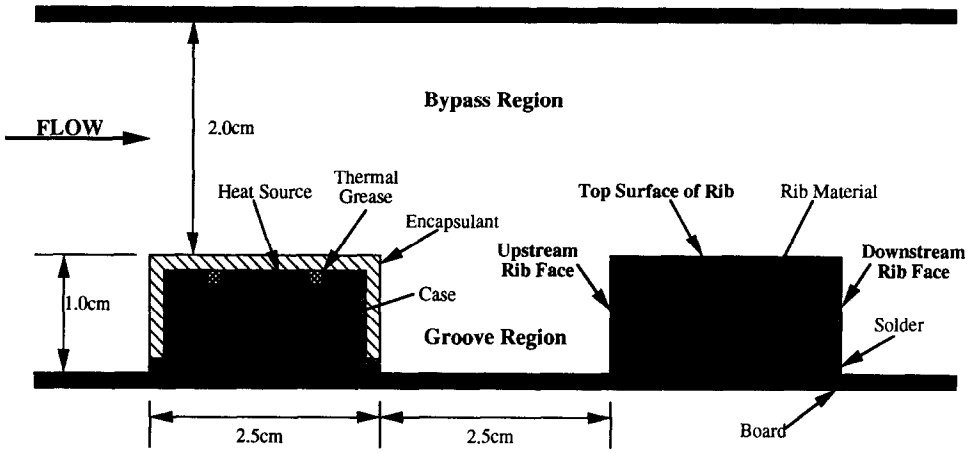

Fig. 1. Schematic of grooved channel and material configurations.

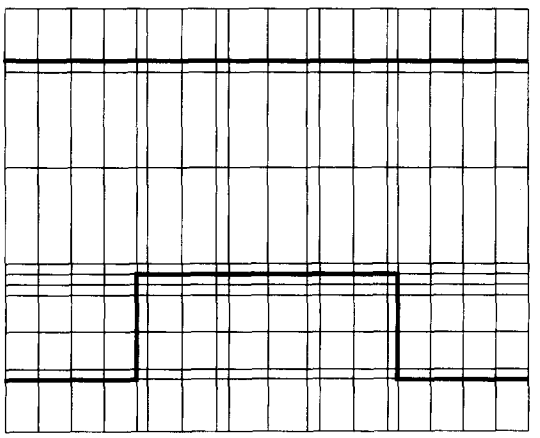

(a)

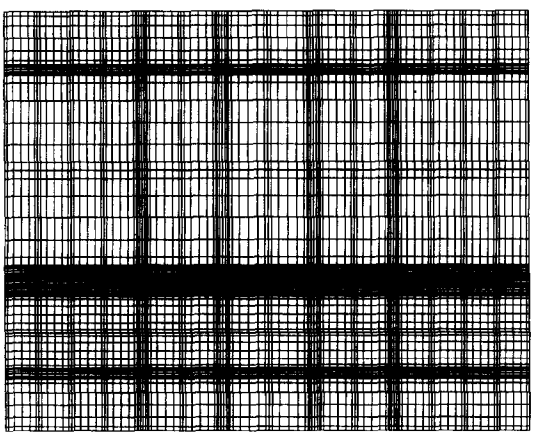

(b)

Fig. 2. Spatial discretization showing (a) macro-elements and (b) collocation points. Darker lines indicate solid–fluid interfaces.

at $Re = 270$ and a maximum streamwise velocity of 36.5 cm s^{-1}. Convective transport from the upstream and downstream rib faces is hampered by the shear layer, which inhibits direct exchange of heated groove fluid with cooler channel fluid. Additionally, the Poiseuille-like nature of the flow in the channel results in larger shear stresses along the top of the rib than along the upstream or downstream rib faces [17]. These effects cause greater convective resistances along the upstream and downstream faces than along the top surface of the rib.

The middle Reynolds number case corresponds to a slightly transitional flow field. Figure 3(b) displays the contours of the streamfunction for this flow regime at $Re = 640$ and a maximum streamwise velocity of 86.4 cm s^{-1}. Small amplitude oscillations, corresponding to Tollmien–Schlichting waves [21, 22] are present within the channel flow. The amplitude of the velocity components associated with the oscillations is approximately two orders of magnitude smaller than the average streamwise velocity of the channel flow. In spite of the small amplitude of the fluctuations, the nature of the transitional flow pattern results in larger shear stresses along the surfaces of the rib [17]. However, the small magnitude of transverse momentum associated with the traveling waves is insufficient to disrupt the shear layer. Therefore, diffusion remains the dominant mode of energy exchange between the heated groove fluid and cooler channel fluid.

The flow field at the high Reynolds number is significantly different from either the middle or low Reynolds numbers. Figure 3(c) displays the instantaneous contours of the streamfunction corresponding to the transitional flow regime at $Re = 700$ and a maximum streamwise velocity of 94.5 cm s^{-1}. This time-periodic flow contains large-amplitude Tollmien–Schlichting waves in the channel. The magnitude of the velocity fluctuations is approximately one order of magnitude smaller than the average streamwise velocity of the channel flow. The increased transverse momentum of the channel flow results in the shear layer being periodically disrupted. Therefore, heated groove fluid can convect into the channel and be replaced by cooler fluid. Additionally, the shear stress along all of the rib surfaces increases significantly,

Table 1. Material properties of the solid domain

Component	k [W cm^{-1} °C^{-1}]	ρc_p [kJ cm^{-3} °C^{-1}]	u''' [W cm^{-3}]
Case	2.04×10^{-1}	3.47	—
Heat source	1.25×10^{-2}	1.74	5.1842
Encapsulate	6.99×10^{-3}	3.16	—
Board	7.4×10^{-3}	2.27	—
Rib material	1.25×10^{-2}	1.74	1.558×10^{-1}
Solder	1.0×10^{-3}	1.47	—
Thermal grease	9.614×10^{-3}	1.71	—
Air	2.851×10^{-4}	1.534×10^{-4}	—

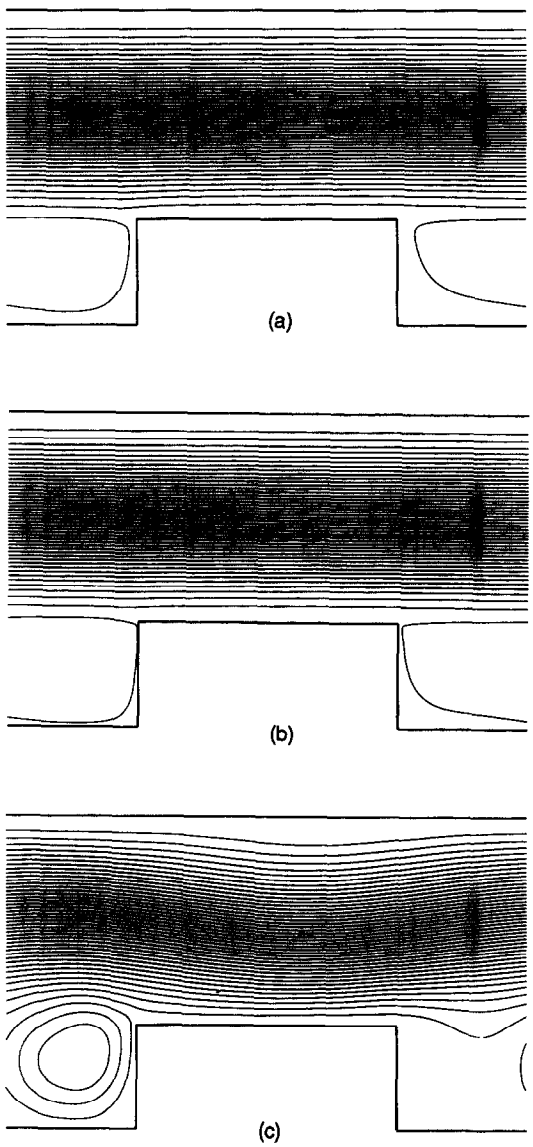

Fig. 3. Contours of the streamfunction for (a) laminar, (b) slightly-transitional, and (c) transitional flow regimes.

which reduces the convective resistance, particularly near the upstream rib corner [17].

SPATIAL DISTRIBUTIONS AT THE SOLID–FLUID INTERFACE

Temperature

Firstly, the local temperatures along the solid–fluid interface of the grooved surface are presented for each of the four configurations and for the three Reynolds numbers studied. The data presented for the middle and high Reynolds number cases are the time-average difference between the solid–fluid interface and bulk-mean temperatures, corresponding to the passing of one Tollmien–Schlichting wave. Additionally, the application of periodic boundary conditions emulates studying the thermal characteristics of heated ribs within the periodic fully-developed region. In this region, the difference between the solid–fluid interface and bulk-mean temperatures remains periodically invariant. Periodic fully-developed behavior has been experimentally observed in similar geometries, e.g. ribbed channels, after the third or fourth component [23, 24].

The interface temperature distributions for all of the cases and configurations exhibit effects associated with both rib material composition and distribution of heat generation, as shown in Fig. 4(a)–(c). For the configurations containing local heat generation, the heat source is positioned near the top of the rib. This results in a local rise of surface temperature directly above the location of the chip.

As the Reynolds number is increased, the convective resistance is lowered near the upstream corner of the rib. However, because of conduction within the solid, variations in the interface temperature distribution are visible along portions of the top and upstream rib faces [Fig. 4(b) and (c)]. The configurations corresponding to single-material composition have lower conductive resistance and exhibit a more asymmetric surface temperature distribution than those with multimaterial composition. This larger conductive resistance localizes convective effects, resulting in larger gradients, but more symmetric overall temperature distributions.

For the high Reynolds number case [Fig. 4(c)], the magnitude of convective transport is large enough to

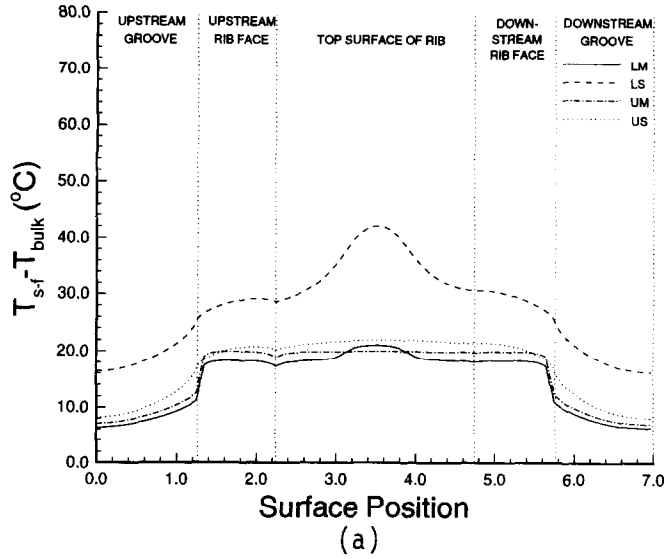

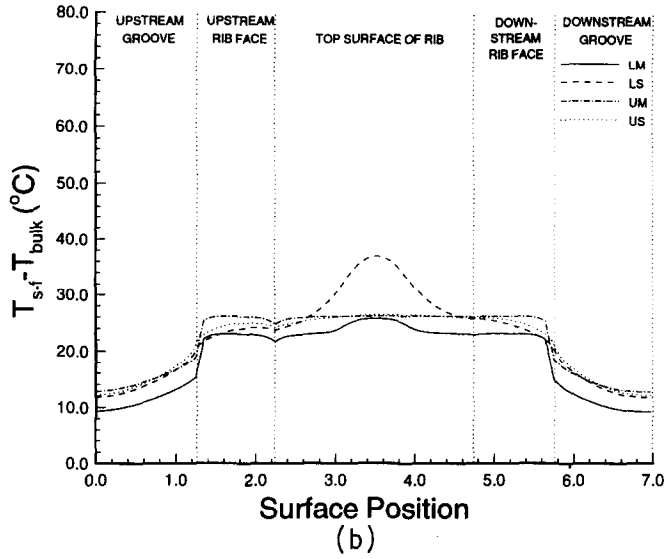

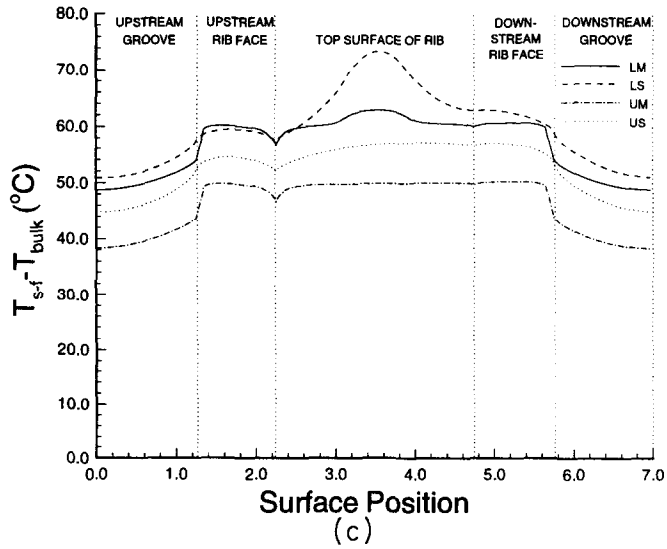

Fig. 4. Solid–fluid interface and bulk-mean temperature difference vs surface position for (a) low, (b) middle, and (c) high Reynolds number cases. LM: local heat generation, multimaterial configuration; LS: local heat generation, single-material configuration; UM: uniform heat generation, multimaterial configuration; and US: uniform heat generation, single-material configuration.

strongly affect the surface temperature distribution for the single-material rib configurations. In fact, the higher rate of convective transport at the leading edge of the rib results in a decrease of surface temperature along nearly 60% of the top surface of the rib for the uniform heat generating, single-material (US) configuration.

Heat flux

The local heat flux distributions are now considered for the same configurations and Reynolds numbers previously examined. As with the interface temperature distributions, the local heat flux data presented for the middle and high Reynolds number cases are time averaged over one wave cycle. Additionally, a sign convention is adopted such that heat flux leaving the solid domain at the solid–fluid interface is positive, while heat flux entering is negative.

The spatial distributions of heat flux for the three Reynolds number cases are displayed in Fig. 5(a)–(c). As previously demonstrated, both material composition and distribution of heat generation affect the resulting patterns. All the configurations display the classical pattern associated with boundary layer growth along the top surface of the rib. However, the configurations with local heat generation display increased heat flux over the location of the heat source. This increase is especially significant for the single-material configuration (LS).

A local increase in heat flux for the multimaterial configurations (LM, UM) occurs along both the upstream and downstream rib faces corresponding to the location of the solder. This is attributable to the larger conductive resistance associated with the solder. The relative convective resistance from the rib face decreases with respect to the conductive resistance into the board, resulting in a local increase of heat flux.

At the low Reynolds number, there is an intact shear layer separating the groove fluid from the channel fluid. The recirculating fluid within the groove is heated along both the upstream and downstream rib faces, but the shear layer prohibits convective exchange of the heated groove fluid with cooler channel fluid. The heated groove fluid becomes hotter than the adjacent surface (board), leading to heat transfer into, rather than out of, the solid domain. However, as the flow becomes transitional and the shear layer is disrupted, some of the heated groove fluid is replaced by cooler channel fluid. This convective exchange of fluid between the groove and channel reduces the magnitude of the temperature gradient along the groove, leading to less heat flux into the solid domain for the higher Reynolds number case. An important observation is that the spatial distribution of flux along the groove surface is affected more by the distribution of heat generation than by the material composition of the rib.

As the Reynolds number increases [Fig. 5(b) and (c)], the peak value of heat flux at the leading edge of the rib increases for all configurations. However, the magnitude of heat flux along the latter portion of the top surface of the rib is reduced for the local heat generating configurations. The increased heat flux along the top of the rib, from the upstream corner to the location of the heat source, raises the temperature of the fluid in the thermal boundary layer. This increases the convective resistance in the streamwise direction, resulting in a reduction of heat flux from the later portion of the rib.

Nusselt number

A classical measure of convective heat transfer is the Nusselt number, which can be interpreted as representing either the nondimensional temperature gradient at the solid–fluid interface or the magnitude of the convective heat transfer scaled by the equivalent conductive heat transfer in the fluid. However, for conjugate problems, the former interpretation is preferable, because it more easily accommodates the presence of both positive and negative heat fluxes along a surface.

The spatial distributions of Nusselt numbers are shown in Fig. 6(a)–(c). Unlike the interface temperature or heat flux distributions, the magnitudes of the Nusselt number for all of the configurations are similar, but the spatial distributions are slightly different. The local heat generating configurations (LS, LM) display increases in Nusselt number above the location of the heat source. Likewise, along the upstream and downstream rib faces, the multimaterial configurations (LM, UM) display increases in Nusselt number over the regions corresponding to the location of the solder. However, there is some disparity in the distribution along the groove. The distributions corresponding to the multimaterial configurations (LM, UM) closely follow one another, particularly along the downstream portion of the groove. However, the single-material configurations (LS, US) do not correlate well along the upstream portion of the groove for the high Reynolds number case. The poor correspondence is associated with the larger amount of heat flux removed from the upstream rib face for the uniform heat generating case (US), after the shear layer is disrupted.

A closer inspection of the distribution along the top surface of the rib reveals a degradation in performance for the local heat generating configurations (LS, LM) after the location of the heat source, especially so for the single-material configuration (LS). As previously described, the fluid within the near-wall portion of the thermal boundary layer is heated along the rib, increasing its convective resistance, as evidenced in the Nusselt number distribution.

Although greater amounts of heat flux are achieved as the Reynolds number is increased, no comparable increases are reflected in the Nusselt number distribution [Fig. 6(b) and (c)]. Furthermore, the variations in spatial distributions along the rib diminish such that the only significant difference for all, save

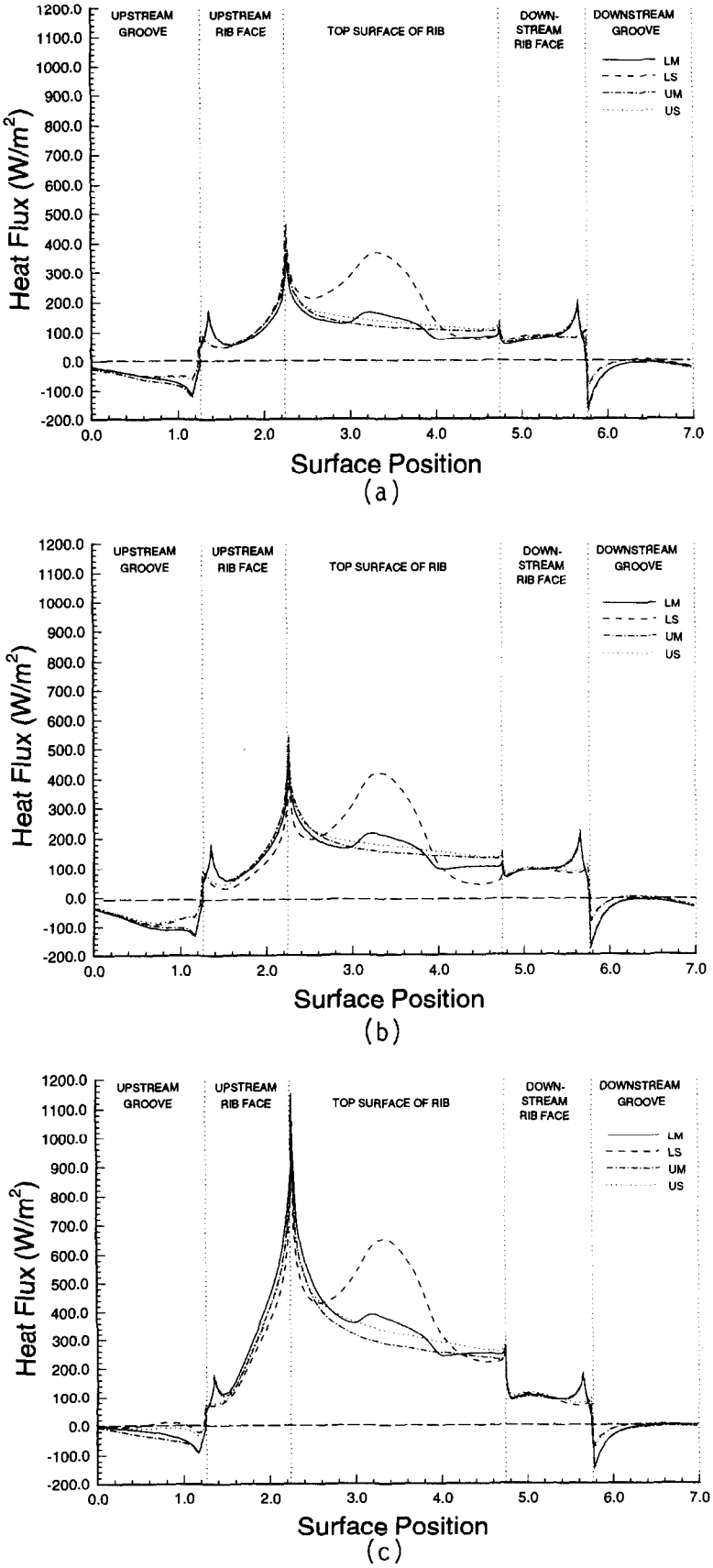

Fig. 5. Heat flux at the solid–fluid interface vs surface position for (a) low, (b) middle, and (c) high Reynolds number cases.

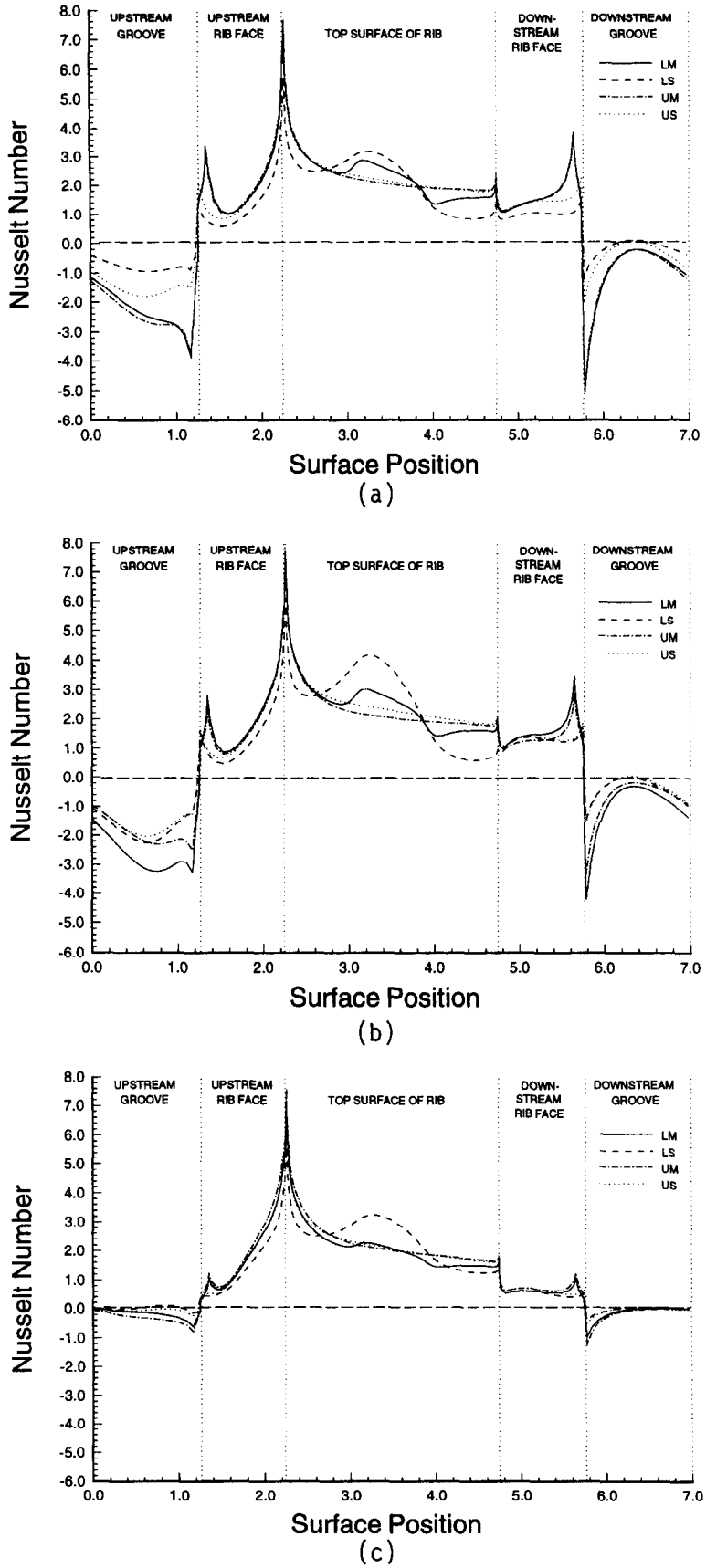

Fig. 6. Nusselt number at the solid–fluid interface vs surface position for (a) low, (b) middle, and (c) high Reynolds number cases.

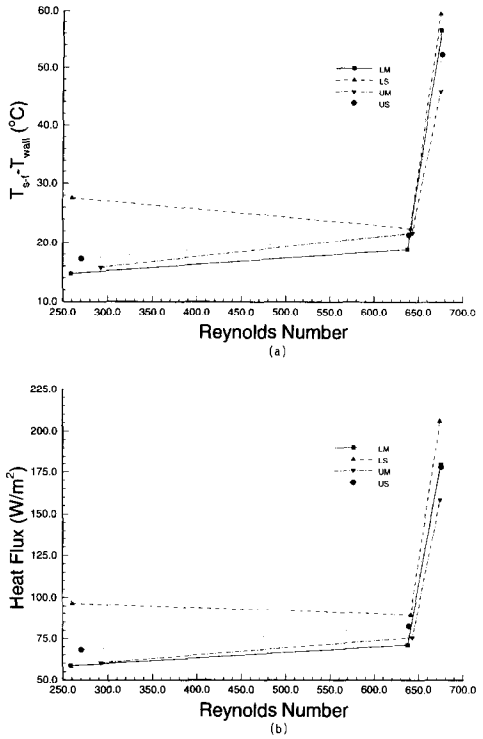

Fig. 7. Time- and space-average (a) difference between the solid–fluid interface and bulk-mean temperatures, and (b) heat flux at the solid–fluid interface vs Reynolds number.

the uniform heat generating single-material rib configuration (US), occurs above the location of the solder and the heat source. However, even the magnitude of these differences is minimized. With increasing Reynolds number, the fluid becomes better mixed, resulting in a more homogeneous thermal distribution within the flow. Therefore, differences in thermal performance caused by upstream variations in heat flux would decrease in significance.

DISCUSSION

Although there are distinct spatial variations of surface temperature, heat flux and Nusselt number within and between the four configurations, more general behavior differences become apparent when spatially-averaged values are examined.

The averaged difference between the local solid–fluid interface and bulk-mean temperatures, as a function of Reynolds number, is shown in Fig. 7(a). The temperature difference for the local heat-generating, single-material rib (LS) decreases with Reynolds number in the subcritical regime. At the high Reynolds number case, the flow becomes more homogeneous and the temperature difference increases. However, the temperature difference for the other configurations continuously increases with Reynolds number, regardless of the flow regime. The key to understanding this behavior is the recognition of the relationship between the temperature rise of the fluid and the heat flux for conjugate problems.

An order of magnitude analysis of the convective boundary condition corresponding to a uniform heat flux at the solid–fluid interface yields an inverse relationship between the heat transfer coefficient and the temperature difference:

$$h(T_{s-f}-T_{bulk}) = -k_s\frac{\partial T_s}{\partial \mathbf{n}} = Q \tag{4a}$$

$$h \propto \frac{1}{(T_{s-f}-T_{bulk})}. \tag{4b}$$

The well-known solution for convective heat transfer over a flat plate, with an imposed uniform heat flux boundary condition, states that the heat transfer coefficient is proportional to the Reynolds number to the one-half power. Therefore, the inverse relationship shown in equation (4b) implies that as the Reynolds number is increased, the wall temperature approaches the bulk-mean temperature. This behavior has also been demonstrated for convective heat transfer from a grooved channel with an imposed uniform heat flux boundary condition [16]. However, an order of magnitude analysis for the conjugate boundary condition reveals a different relationship:

$$k_s\frac{\partial T_s}{\partial \mathbf{n}} = k_f\frac{\partial T_f}{\partial \mathbf{n}} \tag{5a}$$

$$Q = -k_s\frac{\partial T_s}{\partial \mathbf{n}} \sim -\frac{k_f}{H}(T_{s-f}-T_{bulk}) \tag{5b}$$

$$Q \propto (T_{s-f}-T_{bulk}) \tag{5c}$$

namely, the difference between the solid–fluid interface and bulk-mean temperatures is directly proportional to the heat flux [equation (5c)]. As predicted, the spatially-averaged heat flux, displayed in Fig. 7(b), exhibits the same behavior characteristics as the temperature difference.

Physically, energy convected from the rib surface into the fluid increases its bulk-mean temperature. However, when there is little transverse mixing in the flow, the heat removed from the rib results in a non-homogeneous temperature distribution. Therefore, the temperature distribution within the fluid depends upon the spatial distribution of heat flux along the solid–fluid interface and the flow patterns. The local heat generating, single-material configuration [LS, Figs. 5 and 7(b)] exhibits significantly higher heat flux from the top surface of the rib than the other configurations. This distribution of heat flux raises the fluid temperature within the boundary layer above the rib more than for the other configurations. The thermal wake that extends from the preceding rib increases the convective resistance along the top surface of the rib, reducing convective rates. Therefore, until the local flow patterns produce a more homogeneous temperature distribution within the fluid, the difference between the solid–fluid interface and bulk-

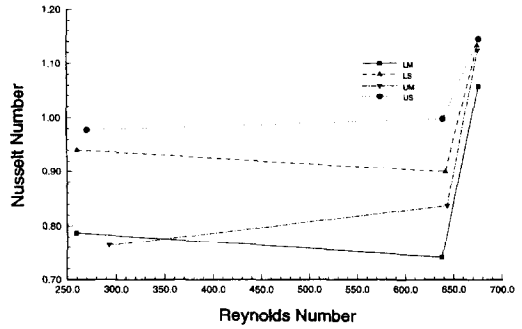

Fig. 8. Time- and space-average Nusselt number vs Reynolds number.

mean temperatures will be larger for this configuration than for the others.

For the high Reynolds number case, the channel flow becomes non-parallel and the shear layer is disrupted, increasing significantly the heat flux along the upstream and downstream rib faces, especially for the uniform heat generating configurations (US, UM). The periodic disruption of the shear layer convects the heated fluid from the groove into the channel. This heated fluid is convected further into the channel, resulting in a lower temperature rise in the fluid directly adjacent to the rib. However, the increased conductive resistance within the multimaterial configurations (LM, UM) reduces the amount of flux removed from the upstream and downstream rib faces. Therefore, the distribution of heat generation dictates the qualitative behavior while the material composition dictates the quantitative performance.

Next, the spatially-averaged Nusselt number is considered as a function of the Reynolds number in Fig. 8. The effect of convective resistance along the top surface of the rib is visible in the spatially-averaged Nusselt number. The spatially-averaged Nusselt number for the local heat generating configurations (LS, LM) decreases with Reynolds number in the subcritical regime and then increases, once the flow becomes supercritical and better mixed. However, the spatially-averaged Nusselt number for the uniform heat generating configurations (US, UM) continuously increases with Reynolds number due to the spatial distribution of heat flux, as previously described.

The uniform heat generating, single-material configuration (US) displays the closest behavior to a nonconjugate analysis, followed by the uniform heat generating, multimaterial configuration (UM). Qualitatively, problems which involve complex flow behavior, including time- and spatially-dependent separation and reattachment, as well as intense heat transfer, multimaterial solid domains and localized heat generation require conjugate formulations. This insight is required for the successful construction of heat transfer correlations for conjugate heat transfer problems. It also indicates that the construction of such correlations might be an exceedingly difficult task for systems that exhibit strong conjugate effects and nonmonotonic relationships with respect to Reynolds number.

CONCLUSIONS

Conjugate conduction/convection heat transport from a grooved channel is investigated for single and multimaterial configurations, as well as for local and uniform distributions of heat generation. At the solid–fluid interface of the grooved surface, the spatial distributions of temperature, heat flux and Nusselt number exhibit variations associated with both material composition and distribution of heat generation. Furthermore, heat fluxes from the cooling fluid to solid regions along some portions of the grooved channel are obtained and, consequently, negative Nusselt numbers for the configurations and Reynolds numbers explored.

Thermal energy, convected from the top surface of the rib, creates a thermal wake that extends downstream. The lack of small scale mixing within the fluid, in these transitional flow regimes, results in incomplete homogenization of the thermal wake causing increased convective resistance along the top surface of the following rib. This resistance is found to be more strongly influenced by the distribution of internal heat generation than by the material composition.

Acknowledgements—We gratefully acknowledge the National Science Foundation support by CTS-8908808 and CTS-9311072, the Engineering Design Research Center, and the Cray computational resources provided by NASA Lewis Research Center and Pittsburgh Supercomputing Center.

REFERENCES

1. T. L. Perelman, On conjugate problems of heat transfer, *Int. J. Heat Mass Transfer* **3**, 293–303 (1961).
2. A. V. Luikov, V. A. Aleksashenko and A. A. Aleksashenko, Analytical methods of solution of conjugated problems in convective heat transfer, *Int. J. Heat Mass Transfer* **14**, 1047–1056 (1971).
3. P. Payvar, Convective heat transfer to laminar flow over a plate of finite thickness, *Int. J. Heat Mass Transfer* **20**, 431–433 (1977).
4. R. Karvinen, Some new results for conjugated heat transfer in a flat plate, *Int. J. Heat Mass Transfer* **21**, 1261–1264 (1978).
5. A. V. Luikov, Conjugate convective heat transfer problems, *Int. J. Heat Mass Transfer* **17**, 257–365 (1974).
6. T. A. Rizk, C. Kleinstreuer and M. N. Ozisik, Analytic solution to the conjugate heat transfer problem of flow past a heated block, *Int. J. Heat Mass Transfer* **35**, 1519–1525 (1992).
7. J. S. Lim, A. Bejan and J. H. Kim, The optimal thickness of a wall with convection on one side, *Int. J. Heat Mass Transfer* **35**, 1673–1679 (1992).
8. A. Brosh, D. Degani and S. Zalmanovich, Conjugated heat transfer in a laminar boundary layer with heat source at the wall, *J. Heat Transfer* **104**, 90–95 (1982).
9. K. D. Cole and J. V. Beck, Conjugated heat transfer from a strip heater with the unsteady surface element method, *AIAA J. Thermophys.* **1**, 348–354 (1987).
10. K. D. Cole and J. V. Beck, Conjugated heat transfer

from a hot-film probe for transient air flow, *J. Heat Transfer* **110,** 290–296 (1988).
11. A. Campo and C. Schuler, Heat transfer in laminar flow through circular tubes accounting for two-dimensional wall conduction, *Int. J. Heat Mass Transfer* **31,** 2251–2259 (1988).
12. J. Davalath and Y. Bayazitoglu, Forced convection cooling across rectangular blocks, *J. Heat Transfer* **109,** 321–328 (1987).
13. A. Zebib and Y. K. Wo, A two-dimensional conjugate heat transfer model for forced air cooling of an electronic device, *J. Electron. Packaging* **111,** 41–45 (1989).
14. J. R. Culham, T. F. Lemczyk, S. Lee and M. M. Yovanovich, META—a conjugate heat transfer model for air cooling of circuit boards with arbitrarily located heat sources. In *Heat Transfer in Electronic Equipment*, Vol. 171, pp. 117–126. ASME Heat Transfer Division, New York (1991).
15. S. Ray and J. Srinivasan, Analysis of conjugate laminar mixed convection cooling in a shrouded array of electronic components, *Int. J. Heat Mass Transfer* **35,** 815–822 (1992).
16. J. S. Nigen and C. H. Amon, Conjugate forced convective effects of time dependent recirculating flows in grooved channels. In *Fundamentals of Forced Convection Heat Transfer* (Edited by M. A. Ebadian and P. H. Oosthuizen), Vol. 210, pp. 91–98. ASME Heat Transfer Division, New York (1992).
17. J. S. Nigen and C. H. Amon, Time-dependent conjugate heat transfer characteristics of self-sustained oscillatory flows in a grooved channel, *ASME J. Fluid Engng* **116,** 499–507 (1994).
18. A. T. Patera, A spectral element method for fluid dynamics: laminar flow in a channel expansion, *J. Comput. Phys.* **54,** 468–488 (1984).
19. C. H. Amon, Spectral element-Fourier method for transitional flows in complex geometries, *AIAA J.* **31,** 42–48 (1993).
20. M. M. Yovanovich and V. W. Antonetti, Application of thermal contact resistance theory to electronic packages. In *Advances in Thermal Modeling of Electronic Components and Systems* (Edited by A. Bar-Cohen and A. D. Kraus), Vol. 1, pp. 79–128. Hemisphere, New York (1988).
21. N. K. Ghaddar, K. Z. Korczak, B. B. Mikic and A. T. Patera, Numerical investigation of incompressible flow in grooved channels. Part 1. Stability and self-sustained oscillations, *J. Fluid Mech.* **163,** 99–127 (1986).
22. C. H. Amon and A. T. Patera, Numerical calculation of stable three-dimensional tertiary states in grooved-channel flow, *Phys. Fluids A* **1,** 2001–2009 (1989).
23. G. L. Lehmann and R. A. Wirtz, The effect of variations in stream-wise spacing and length on convection from surface mounted rectangular components. In *Heat Transfer in Electronic Equipment*, Vol. 48, pp. 39–47. ASME Heat Transfer Division, New York (1985).
24. S. V. Garimella and P. A. Eibeck, Heat transfer characteristics of an array of protruding elements in single phase forced convection, *Int. J. Heat Mass Transfer* **33,** 2659–2669 (1990).